JACS
JOURNAL OF THE AMERICAN CHEMICAL SOCIETY
Article
pubs.acs.org/JACS

Hierarchical Self-Organization of Perylene Bisimides into Supramolecular Spheres and Periodic Arrays Thereof

Dipankar Sahoo,[†,‡] Mihai Peterca,[†,‡] Emad Aqad,[†] Benjamin E. Partridge,[†] Paul A. Heiney,[‡] Robert Graf,[§] Hans W. Spiess,[§] Xiangbing Zeng,[¶] and Virgil Percec*[,†]

[†]Roy & Diana Vagelos Laboratories, Department of Chemistry, University of Pennsylvania, Philadelphia, Pennsylvania 19104-6323, United States

[‡]Department of Physics and Astronomy, University of Pennsylvania, Philadelphia, Pennsylvania 19104-6396, United States

[§]Max-Planck Institute for Polymer Research, 55128 Mainz, Germany

[¶]Department of Materials Science and Engineering, University of Sheffield, Sheffield S1 3JD, United Kingdom

Supporting Information

ABSTRACT: Perylene bisimide derivatives (PBIs) are known to form only columnar or lamellar assemblies. There is no known example of a PBI self-assembling into a supramolecular sphere. Therefore, periodic and quasiperiodic arrays generated from spherical assemblies produced from PBIs are also not known. Here, a PBI functionalized at its imide groups with a second generation self-assembling dendron is reported to self-assemble into supramolecular spheres. These spheres self-organize in a body-centered cubic (BCC) periodic array, rarely encountered for self-assembling dendrons but often encountered in block copolymers. These supramolecular spheres also assemble into a columnar hexagonal array in which the supramolecular columns are unexpectedly and unprecedentedly made from spheres. At lower temperature, two additional columnar hexagonal phases consisting of symmetric and asymmetric tetrameric crowns of PBI are observed. Structural and retrostructural analysis via X-ray diffraction (XRD), molecular modeling, molecular simulation, and solid state NMR suggests that inversion of the symmetric tetrameric crowns at high temperature mediates their transformation into supramolecular spheres. The tetrameric crowns of PBIs are able to form an isotropic sphere in the cubic phase due to rapid molecular motion at high temperature, unobservable by XRD but demonstrated by solid state NMR studies. This mechanism of hierarchical self-organization of PBI into supramolecular spheres is most probably general and can be applied to other related planar molecules to generate new functions.

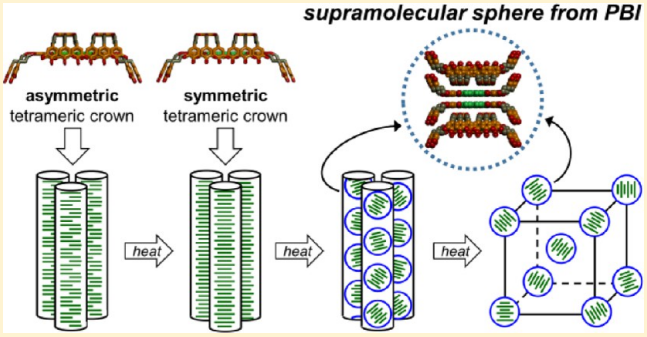

INTRODUCTION

Substituted perylene bisimides (PBIs) are an archetypal[1a] building block for supramolecular assemblies,[1] both due to the ease with which they can be synthetically tailored and due to the wide range of their potential applications, most recently including biologically relevant assemblies[2] and organic electronics.[3] The large, planar aromatic core of PBI facilitates cofacial $\pi-\pi$ stacking,[1a] favoring columnar[4,5] and lamellar[1a] assemblies. Although 3D phases generated from spheres, including $Pm\bar{3}n$ cubic,[6] $Im\bar{3}m$ body-centered cubic (BCC),[7] $P4_2/mnm$ tetragonal,[8] and 12-fold liquid quasicrystalline (LQC),[9] have been discovered for self-assembling dendrons and recently transplanted to block copolymers,[10] surfactants,[11] and other soft matter,[12] no such phases have ever been observed for an assembly of PBI, presumably due to the inability of the PBI geometry to generate a suitable spherical building block. Micelles and hollow vesicular structures assembled from PBI derivatives have been obtained via coassembly in solution.[13] However, vesicles exhibit different shapes and broad polydispersity, and represent lamellar structures with substantial curvature. Therefore, they do not self-organize into periodic arrays, a requirement to demonstrate a perfectly spherical building block.

Library approaches developed in our laboratory[1b,14] have demonstrated that spherical building blocks are generated from a single spherical molecule[6b] or from assemblies of molecules with either a conical[6a,8] or crown[15] conformation. Here we report the synthesis, structural, and retrostructural analysis[1b,14] of a PBI dendronized at its imide groups with two identical second generation dendrons (denoted G2-PBI) that assembles into a supramolecular sphere generated from tetrameric crowns (TCs). These supramolecular spheres of G2-PBI further organize into an $Im\bar{3}m$ BCC lattice at high temperature and, upon cooling, into a columnar hexagonal phase in which supramolecular columns are themselves made from spheres.

Received: September 22, 2016
Published: October 19, 2016

DOI: 10.1021/jacs.6b09986
J. Am. Chem. Soc. 2016, 138, 14798−14807

Symmetric and inverted TCs are responsible for the formation of the supramolecular sphere and subsequent organization into both a cubic phase and a columnar hexagonal phase generated from columns of spheres, whereas symmetric and asymmetric TCs enable two classical columnar hexagonal phases at lower temperature. The rapid molecular motion of the TCs of G2-PBI at elevated temperature enables this first example of a spherical building block assembled from PBI.

RESULTS AND DISCUSSION

Synthesis of Perylene Bisimide with Second Generation Self-Assembling Dendrons, G2-PBI. The synthesis of G2-PBI dendronized with second generation benzyl ether dendrons is shown in Scheme 1.

Scheme 1. Synthesis of G2-PBI[ab]

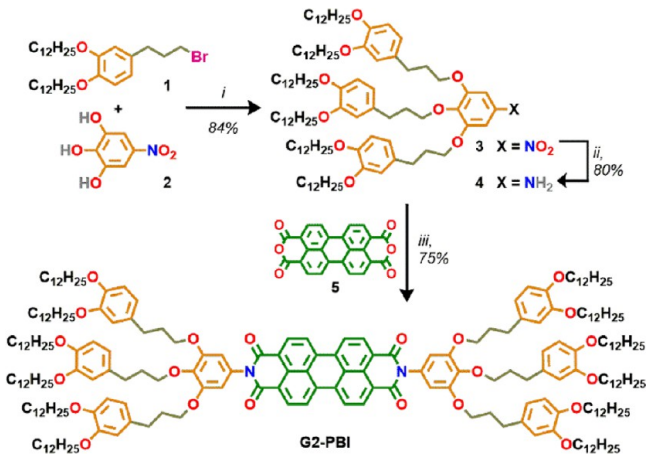

[a]Reagents and conditions: (i) Dry K_2CO_3, DMF, 75 °C, 16 h; (ii) $N_2H_4{\cdot}H_2O$, EtOH/THF, reflux, 15 h; (iii) 5, $Zn(OAc)_2{\cdot}2H_2O$, quinoline, 180 °C, 8 h. [b]Color code (also used in all models): Br, pink; O, red; N, blue; C atoms of the PBI, green; C atoms of phenyl rings, orange; C atoms of the propylene linker, gray; peripheral dodecyl chains, black.

First generation propyl dendron bromide **1**, synthesized as reported,[16] was functionalized with nitrophenol **2**, also prepared by known procedures,[5a] via a Williamson etherification with K_2CO_3 in dry *N*,*N*-dimethylformamide (DMF) to give the second generation dendron 3 in 84% yield. Reduction of the nitro group of **3** with hydrazine hydrate in refluxing ethanol and tetrahydrofuran (THF) gave amine dendron **4** in 80% yield after 15 h. Functionalization of perylene tetracarboxylic dianhydride (**5**) with **4** in the presence of zinc acetate dihydrate in quinoline provided G2-PBI in 75% isolated yield after column chromatography in acetone/DCM (1:20) and precipitation of a dichloromethane (DCM) solution into methanol. Detailed synthetic procedures and complete characterization data are presented in the Supporting Information.

Thermal Analysis by Differential Scanning Calorimetry (DSC). G2-PBI was analyzed by DSC to determine the temperatures at which first order phase transitions occur and the enthalpy changes associated with each transition (Figure 1). Phases indicated in Figure 1 were identified by X-ray diffraction (XRD, to be discussed later).

The as-prepared sample of G2-PBI generates a 3D crystalline columnar hexagonal (Φ_h^k) phase below 7 °C which transitions

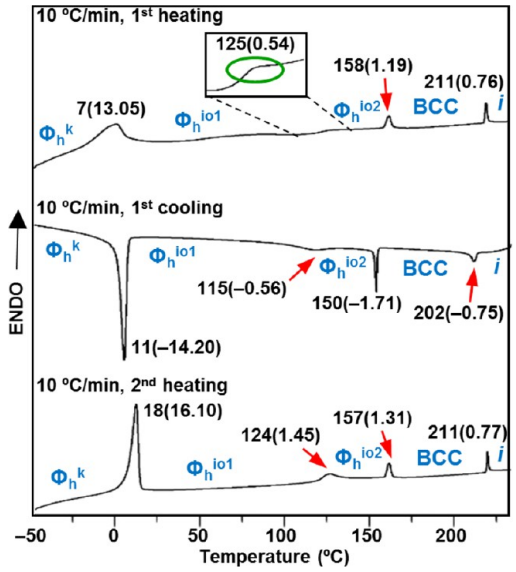

Figure 1. DSC traces of G2-PBI recorded with heating and cooling rates of 10 °C/min upon first heating, first cooling, and second heating. Phases determined by XRD (defined in main text), transition temperatures (in °C), and associated enthalpy changes (in parentheses in kcal/mol) are indicated.

into a 2D liquid crystalline columnar hexagonal phase with intracolumnar order (Φ_h^{io}) at 7 °C. XRD analysis reveals that two distinct 2D Φ_h^{io} phases are generated by G2-PBI upon first heating: a low temperature phase observed between 7 and 125 °C, denoted Φ_h^{io1}, and a high temperature phase observed between 125 and 158 °C, denoted Φ_h^{io2}, all with *P6mm* space group. The 2D Φ_h^{io2} phase transforms into a BCC ($Im\bar{3}m$) phase at 158 °C, which melts into an isotropic liquid at 211 °C. Subsequent cooling and second heating regenerates all four phases (Φ_h^k, Φ_h^{io1}, Φ_h^{io2}, and BCC). The transition temperature upon heating from Φ_h^k to Φ_h^{io1} increases from 7 °C on first heating to 18 °C on second heating, and is accompanied by a substantially sharper thermal transition and higher associated enthalpy change (Figure 1, bottom), suggesting that Φ_h^k generated upon first cooling from Φ_h^{io1} is more highly ordered than that observed in the as-prepared sample. Due to the high viscosity of G2-PBI, thermal optical polarized microscopy does not provide very specific textures that can differentiate clearly between various columnar hexagonal phases, although a small difference between the textures of two columnar hexagonal phases is observed (Supporting Information, Figure SF1). The boundaries between textures of Φ_h^{io1} (Figure SF1a) are sharper and better resolved than those of Φ_h^{io2} (Figure SF1b). Heating into the BCC phase provides a black image, as expected from an optically isotropic phase (Figure SF1c).

Supramolecular Columns Self-Organized from Asymmetric Tetrameric Crowns (TCs). Phases denoted in Figure 1 were determined by analysis of XRD patterns of oriented fibers and powder samples of G2-PBI. XRD data were collected at two different detector-to-sample distances to permit observation of diffraction features arising from different ranges of *d*-spacings: at a distance of 0.54 m, denoted *intermediate-angle X-ray scattering* (IAXS), and at 0.11 m, denoted *wide-angle X-ray scattering* (WAXS). The structures of the supramolecular assemblies comprising each phase were determined by (a) construction of a molecular model, (b) simulation of the XRD pattern of that model using Cerius[2] software, (c) comparison of

DOI: 10.1021/jacs.6b09986
J. Am. Chem. Soc. 2016, 138, 14798–14807

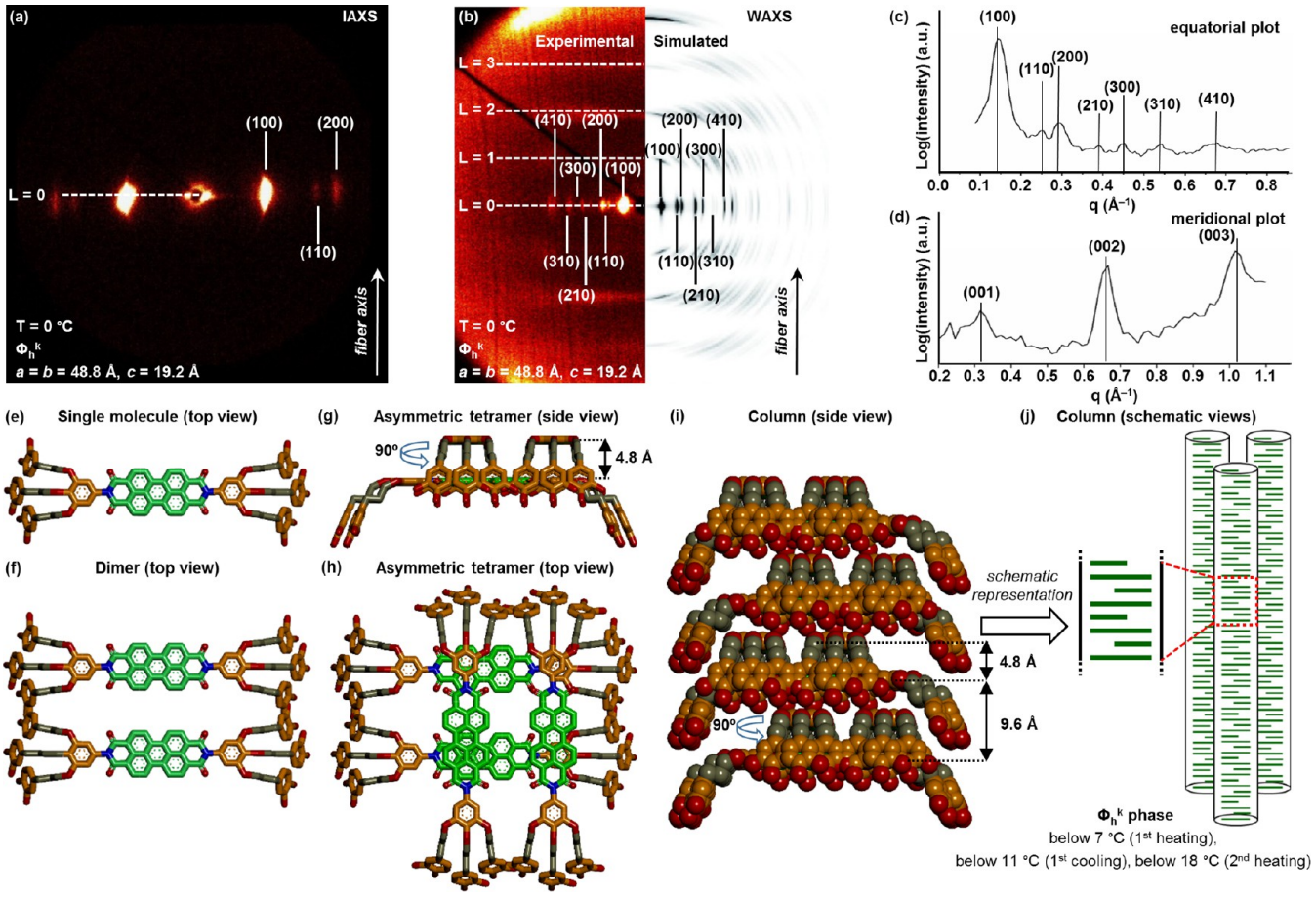

Figure 2. XRD patterns and molecular models of the 3D crystalline columnar hexagonal (Φ_h^k) phase generated from asymmetric tetrameric crowns. Data collected from an oriented fiber during second heating after initial heating to the Φ_h^{io1} phase and cooling to the Φ_h^k phase at 10 °C/min. (a) Experimental IAXS pattern. (b) Experimental WAXS pattern (left) compared with XRD pattern simulated from the model in (e–i) (right). (c, d) Radial plots along (c) equatorial and (d) meridional axes of the WAXS pattern. Temperature, phase, lattice parameters, layer lines and fiber axis are indicated. (e–i) Molecular models of the Φ_h^k phase: (e) single molecule, top view; (f) dimer, top view; (g, h) asymmetric tetrameric crown, (g) side and (h) top view; (i) column, side view. Color code: O, red; N, blue; C atoms of the PBI, green; C atoms of phenyl rings, orange; C atoms of the propylene linker, gray. Peripheral dodecyl ($-C_{12}H_{25}$) chains are omitted for clarity. (j) Schematic representation of columns with molecules indicated as green bars.

the experimental and simulated XRD patterns, and (d) refinement of the molecular model. In selected cases, the X-ray patterns were also compared to models for the orientational distribution of columns using a simulation which performed Fourier transforms of simplified structural models incorporating the necessary disorder. This iterative process was repeated until the experimental XRD pattern was well reproduced by the XRD pattern simulated from the molecular model.

XRD patterns measured upon second heating demonstrate that G2-PBI assembles into a 3D crystalline columnar hexagonal (Φ_h^k) phase at 0 °C (Figure 2). The column axis (lattice *c*-axis) is oriented along the fiber axis.[5] The observation of higher-order Bragg peaks (d_{100}, d_{110}, d_{200}, d_{210}, d_{300}, d_{310}, and d_{410}) in the Φ_h^k phase (Figure 2b,c) indicates a higher degree of ordering on the atomic scale compared to the Φ_h^{io1} phase, in which these higher-order Bragg peaks are not observed (Figure 3), most likely driven by freezing of the aliphatic chains at low temperatures. The large enthalpy change observed by DSC (16.10 kcal/mol at 18 °C upon second heating) upon transition from Φ_h^k to Φ_h^{io1} indicates that Φ_h^k at 0 °C cannot be liquid crystalline. It must therefore be a crystalline columnar hexagonal phase, even though *hkl* diffractions indicative of intercolumnar order are not observed, most probably due to the quenching in of the disorder of the Φ_h^{io1} phase upon cooling.

The number of molecules in each stratum of the supramolecular column, μ, can be determined from the experimental density and the XRD-derived lattice parameters (Table 1). Taking the experimental values for the Φ_h^k phase of G2-PBI, we can calculate that μ = 1.7. Due to experimental error in the density measurement (~5%) and determination of the lattice parameters (~5% per parameter), we can conclude from μ = 1.7 that there are two molecules per column stratum of thickness 4.8 Å. The experimentally derived *c*-parameter further indicates that there are four (c/t = 19.2 Å/4.8 Å = 4) column strata per unit cell, forming a column of diameter, D_{col} (= *a* for Φ_h^k), of 48.8 Å.

A model consistent with the lattice parameters and density calculations described above suggests that each column stratum is formed by two molecules (Figure 2e) whose cores are adjacent and coplanar (Figure 2f). This stratal dimer repeats at an interval of 4.8 Å along the column axis. This $\pi-\pi$ stacking distance of 4.8 Å is larger than the 3.3–3.5 Å close contact stacking typically observed in columnar assemblies of PBI derivatives.[5] In G2-PBI, steric interactions between the hydrogen atoms on the phenyl ring of the dendron and the

DOI: 10.1021/jacs.6b09986
J. Am. Chem. Soc. 2016, 138, 14798–14807

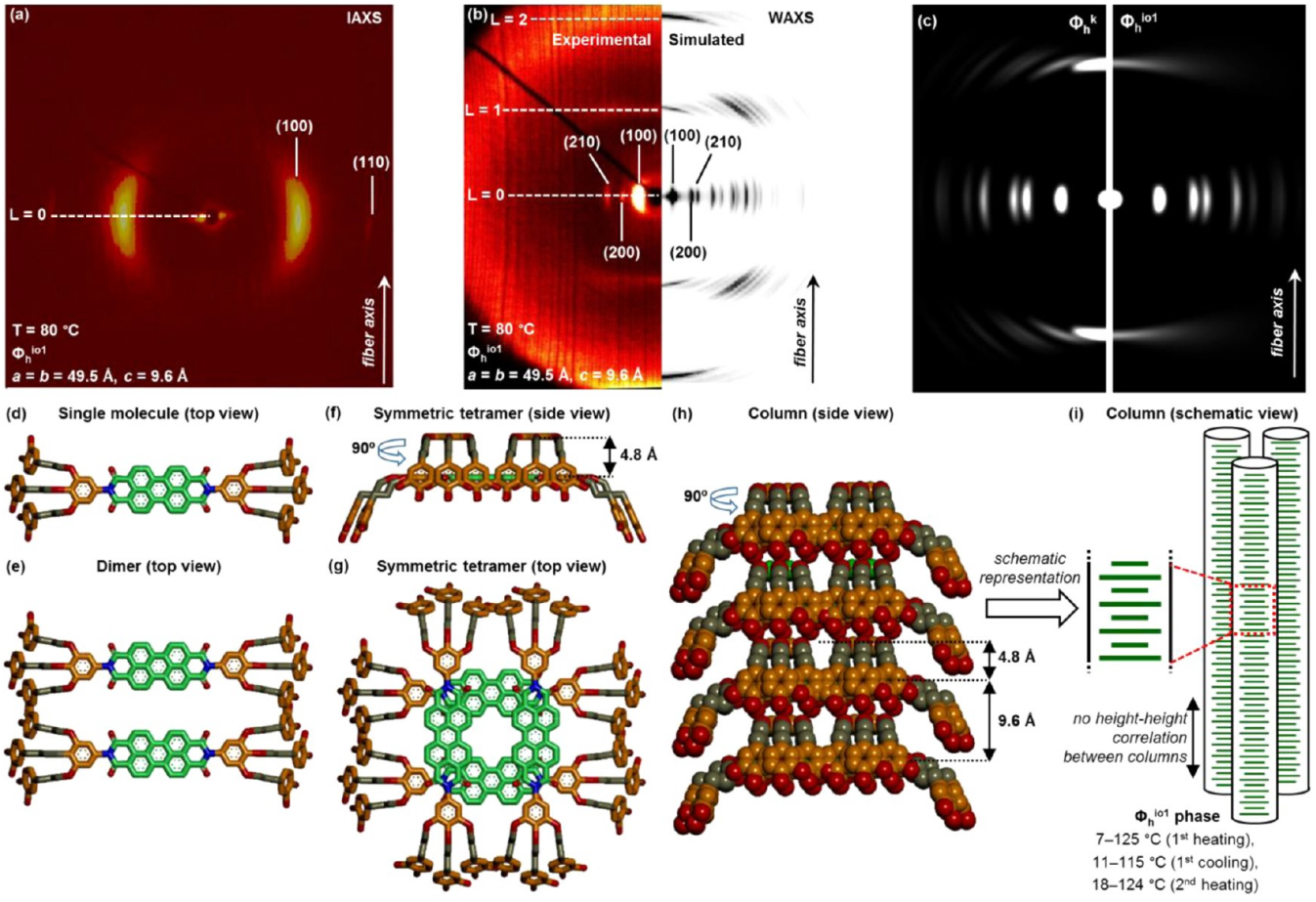

Figure 3. XRD patterns and molecular models of the low temperature 2D liquid crystalline columnar hexagonal phase with intracolumnar order (Φ_h^{io1}) generated from symmetric tetrameric crowns. Data collected from an oriented fiber during first heating at 10 °C/min. (a) Experimental IAXS pattern. (b) Experimental WAXS pattern (left) compared with XRD pattern simulated from the model in (d–h) (right). (c) Simulation of fiber scattering from the (left) Φ_h^{k} and (right) Φ_h^{io1} phases, with intracolumnar positional order but random column heights. Note that (001) and ($hk1$) diffractions are sharp in the simulated pattern of Φ_h^{k}, but ($hk1$) diffractions have been smeared into a streak in Φ_h^{io1}, as observed in the experimental data in (b). Temperature, phase, lattice parameters, layer lines and fiber axis are indicated. (d–h) Molecular models of the Φ_h^{io1} phase: (d) single molecule, top view; (e) dimer, top view; (f, g) symmetric tetrameric crown, (f) side and (g) top view; (h) column, side view. Color code: O, red; N, blue; C atoms of the PBI, green; C atoms of phenyl rings, orange; C atoms of the propylene linker, gray. Peripheral dodecyl ($-C_{12}H_{25}$) chains are omitted for clarity. (i) Schematic representation of columns with molecules indicated as green bars.

Table 1. Structural Analysis of G2-PBI by XRD

T (°C)	phase[a]	a, b, c (Å)[b]	t (Å)[c]	ρ (g/cm^3)[d]	M_{wt} (g mol^{-1})[e]	μ[f]	D_{col} (Å)[g]	d_{100}, d_{110}, d_{200}, d_{210}, d_{300}, d_{310}, d_{410}, d_{001}, d_{002}, d_{003} (Å);[h] d_{110}, d_{200}, d_{211} (Å)[i]
0	Φ_h^{k}	48.8, 48.8, 19.2	4.8	1.02	3559.5	1.7	48.8	42.5, 24.5, 21.2, 16.0, 14.1, 11.7, 9.7, 9.2, 19.2, 9.6, 6.4[h]
80	Φ_h^{io1}	49.5, 49.5, 9.6	4.8			1.8	49.5	42.9, –, 21.5, 16.2, –, –, –, –, 9.6, –, –[h]
140	Φ_h^{io2}	46.1, 46.1, –					46.1	
180	BCC	51.6, 51.6, 51.6					44.7	38.4, 25.9, 21.1[i]

[a]Phase notation: Φ_h^{k}, 3D crystalline columnar hexagonal phase; Φ_h^{io1}, low temperature 2D liquid crystalline columnar hexagonal phase with intracolumnar order; Φ_h^{io2}, high temperature 2D liquid crystalline columnar hexagonal phase with intracolumnar order; BCC, body-centered cubic phase. [b]Lattice parameters calculated using $d_{hk} = (\sqrt{3}a/2)(h^2 + k^2 + hk)^{-1/2}$ for hexagonal phases, and $d_{hkl} = (a)(h^2 + k^2 + l^2)^{-1/2}$ for the cubic phase. [c]Average column stratum thickness calculated from the meridional axis features of WAXS fiber patterns. [d]Experimental density measured at 23 °C. [e]Molecular weight. [f]Average number of dendrimers forming the supramolecular column stratum with thickness t, calculated using $\mu = (N_A A t \rho)(M_{wt})^{-1}$, where $N_A = 6.022 \times 10^{23}$ mol^{-1} = Avogadro's number and A is the area of the column cross section calculated from the lattice parameters. [g]Column diameter for Φ_h phases ($D_{col} = a$) and sphere diameter for the BCC phase ($D_{sphere} = \sqrt{3}a/2$). [h]Experimental d-spacings for the Φ_h phases. [i]Experimental d-spacings for the BCC phase.

oxygen atoms of the bisimide cause a twist of the phenyl ring out of the plane of the aromatic PBI core. This twist precludes close-contact stacking and results in an increased $\pi-\pi$ stacking distance. This mechanism will be discussed in more detail in a future publication. Thus, each dimer is separated by 4.8 Å and rotated by 90° with respect to its neighbor. However, the column axis, about which the dimers are rotated, is not coincident with the center of each dimer. Instead, each dimer is displaced from the center of the column in the *ab*-plane and thus each pair of dimers forms an asymmetric tetramer (Figure

DOI: 10.1021/jacs.6b09986
J. Am. Chem. Soc. 2016, 138, 14798–14807

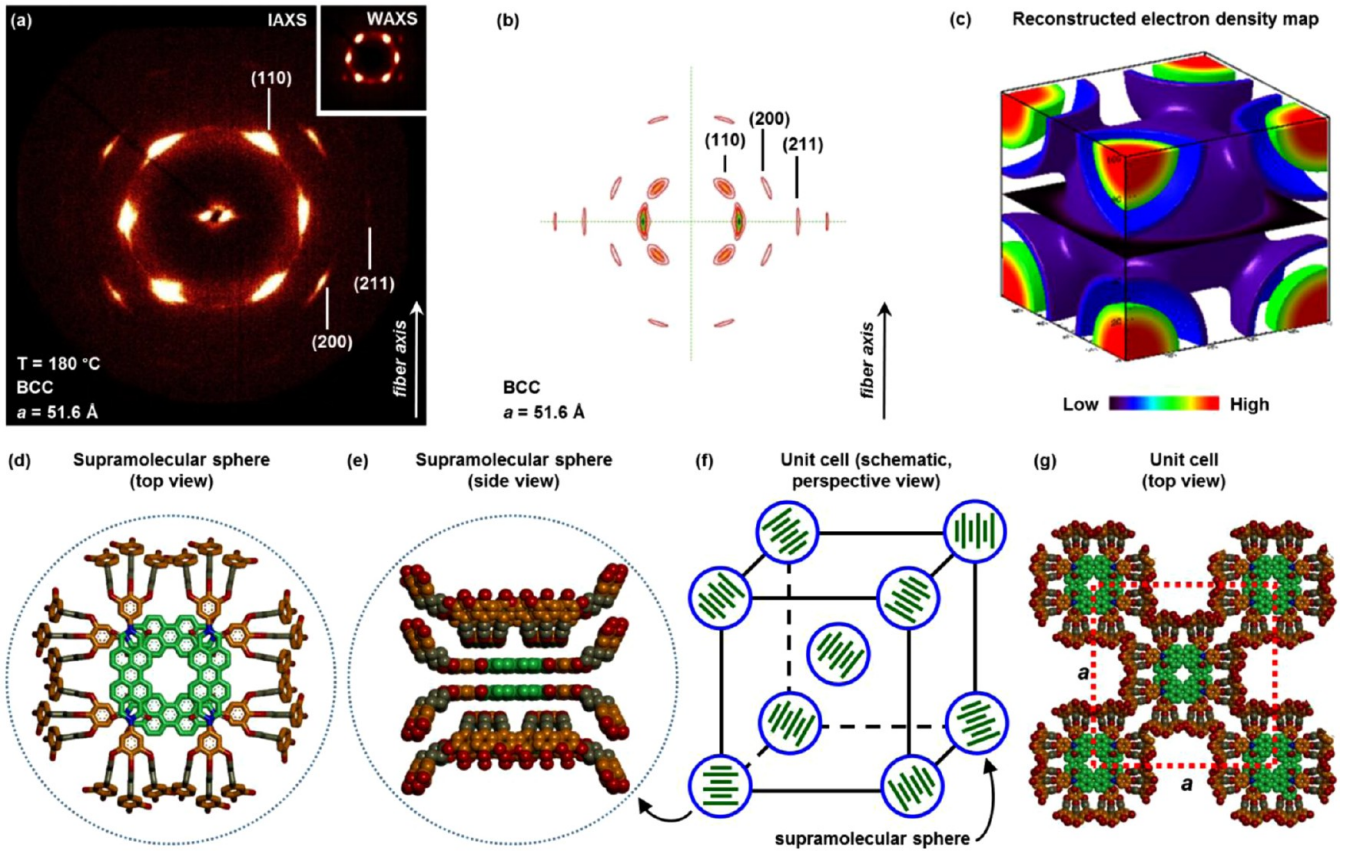

Figure 4. XRD patterns and molecular models of the supramolecular spheres generated from symmetric and inverted tetrameric crowns generating the BCC ($Im\bar{3}m$) array. Data collected from an oriented fiber during first heating at 10 °C/min. Temperature, phase, lattice parameters, and fiber axis are indicated. (a) Experimental IAXS and (inset) WAXS patterns. (b) Molecular simulation assuming BCC packing using the model in (d–g), without orientational disorder of the subunits. The $[111]_{cub}$ axis is aligned with the fiber axis. (c) Reconstructed electron density map. (d–g) Molecular and supramolecular models of the BCC phase. (d) Top and (e) side views of the 12-molecule supramolecular sphere. (f) Schematic view of the BCC unit cell after the structural units have been orientationally averaged to form spheres. (g) Top view of the unit cell. Color code: O, red; N, blue; C atoms of the PBI, green; C atoms of phenyl rings, orange; C atoms of the propylene linker, gray. Red lines in (g) have been used to show the unit cell parameters. Peripheral dodecyl ($-C_{12}H_{25}$) chains are omitted for clarity.

2g,h). The propyl chains in the second generation dendrons, and aliphatic dodecyl chains, enable these tetramers to adopt a crown conformation.[15] These asymmetric tetrameric crowns (TCs) stack along the column axis rotated by 180° with respect to each other such that the resultant column has a repeating unit equal to two TCs, that is, four column strata or eight molecules (Figure 2i). Simulation of the XRD pattern of this model qualitatively reproduces the experimentally observed intensities (Figure 2b). This shifting of molecules and off-centered molecular arrangements to form asymmetric units stacked along the column axis have been observed previously in PBI derivatives.[5c,d]

Supramolecular Columns Self-Organized from Symmetric TCs. The large enthalpy change of the transition between the Φ_h^k and Φ_h^{io1} phases (16.10 kcal/mol upon second heating, Figure 1a) is inconsistent with a phase transition between two hexagonal crystalline phases, but can be explained by the disruption of a crystalline phase to give a liquid crystalline array. The diffraction patterns of G2-PBI observed in Φ_h^{io1} (Figure 3a,b) are consistent with a liquid crystalline columnar hexagonal phase (space group *P6mm*), with extended intracolumnar order but without intercolumnar *height–height* correlations. This intracolumnar order extends over a greater range than a 2D liquid crystal but over a shorter range than a 3D crystalline array. XRD data indicate that the supramolecular column of Φ_h^{io1} has a smaller diameter ($D_{col} = a$) than that of Φ_h^k (49.5 vs 48.8 Å, respectively).

As in Φ_h^k, it can be calculated (Table 1) that there are two molecules (μ = 1.8) per column stratum of thickness 4.8 Å. Molecules of G2-PBI in Φ_h^{io1} form dimers (Figure 3e) identical to those in Φ_h^k (Figure 2f). However, the center of the dimer in Φ_h^{io1} is coincident with the column axis and therefore the supramolecular column has a symmetric TC repeating unit equal to two column strata containing four molecules (Figure 3f,g). The supramolecular columns formed from this symmetric TC of thickness 9.6 Å (Figure 3h) pack into a hexagonal lattice without correlation between the heights of molecules in adjacent columns. Furthermore, the lack of higher order *hk*0 Bragg peaks, such as d_{300}, d_{310}, and d_{410}, in the experimental XRD pattern of the Φ_h^{io1} phase (Figure 3b, left) indicates a degree of disorder in the supramolecular structure, arising perhaps from movement of the supramolecular columns or liquid-like disorder in the aliphatic chains.

Supramolecular Spheres Self-Organized from Symmetric and Inverted Tetrameric Crowns. Both the orientations and radial positions of the diffraction peaks in the XRD patterns of the phase observed between 158 and 211 °C are well described by a BCC phase with a = 51.6 Å (Figure 4a).[7] The BCC lattice has identical structural units at each vertex and at the center of a conventional cubic unit cell

DOI: 10.1021/jacs.6b09986
J. Am. Chem. Soc. 2016, 138, 14798–14807

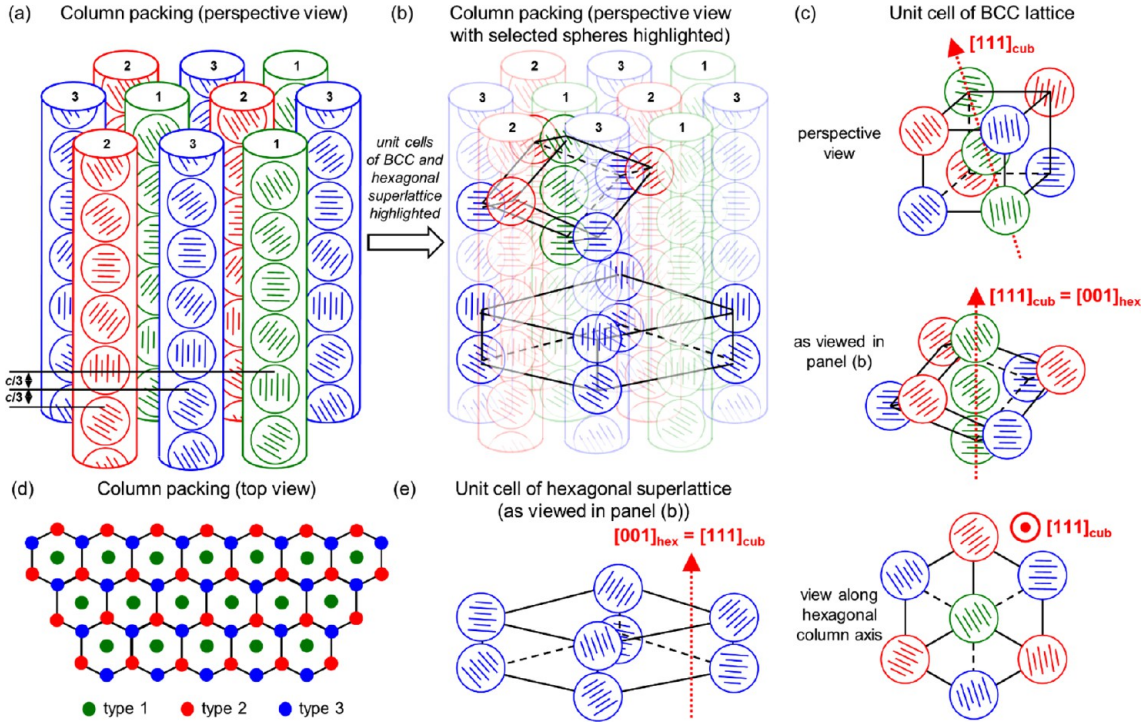

Figure 5. Schematic depiction of a BCC cubic lattice treated as a $\sqrt{3} \times \sqrt{3}$ hexagonal lattice (Φ_h^{io} phase). The "spheres" are the 12-molecule subunits shown in Figure 4d,e. The distance between spheres in each column is c. The lattice a-parameter is the distance between identical columns, $a = c\sqrt{(8/3)}$. Spheres within columns 1, 2, and 3 are displaced along the column axis by $z = 0$, $z = c/3$, and $z = 2c/3$, respectively.

(Figures 4f and 5). The BCC lattice observed here most likely belongs to space group $Im\bar{3}m$ in agreement with previous BCC phases assembled from soft matter.[7] The BCC phase assignment is also supported by the comparable sphere and column diameters (D_{sphere} (BCC, 180 °C) = $(\sqrt{3}/2)a^2$ = 44.7 Å and D_{col} (Φ_h^{io2}, 140 °C) = a = 46.1 Å).[15b]

Electron density maps reconstructed from XRD data (Figure 4c) suggest that the structural subunits are almost uniform spheres of electron density centered at the vertices and center of the conventional BCC cell. The relative intensity profile is dominated by the (110) diffraction, as there is little change to the reconstructed electron density map upon inclusion of the relatively weak (200) and (211) diffractions. From the experimental density and BCC lattice parameters, we calculate that there must be 24 molecules per unit cell, forming two repeat units of 12 molecules each. We initially consider this 12-molecule unit to consist of three TCs (Figures 3f, g and 4e) from the supramolecular column of the Φ_h^{io1} phase. The top and bottom TCs in the supramolecular sphere are symmetric TCs (Figure 3f, g), whereas the central TC is inverted such that the dendrons in each dimer are pointed in opposite directions (Figure 4e). This distorted geometry of the central TC is similar to the planar and saddle-like conformations observed in sphere-forming crowns of dendronized cyclotriveratrylene[15a] and triphenylene.[15b] The supramolecular unit has an orthorhombic shape, but the shape of the surface defined by the ends of the highly disordered aliphatic tails is approximately spherical (Figure 4e).[15,17] This unit is the first example of a supramolecular sphere assembled from PBIs. The BCC lattice is generated by placing one of these spherical orientationally averaged units at each corner and in the center of the cubic cell and hence is a type of "plastic crystal" like the high temperature phase of C_{60}.[18] Solid state NMR (to be discussed later) demonstrates that G2-PBI is very mobile in the cubic phase, suggesting a mechanism via which the supramolecular spheres achieve the orientational disorder required to retain cubic symmetry.

BCC as a Special Case of the Hexagonal Lattice. Extrusion of a fiber preferentially aligns the column axis (lattice c-axis) of the supramolecular columns along the fiber axis. Upon heating to the BCC phase, one of the $[111]_{cub}$ (body diagonal) cubic directions is oriented along the fiber axis, while the other three $[111]_{cub}$ directions are randomly pivoted about that axis. We note here that the 3-fold symmetry of the cubic lattice around the $[111]_{cub}$ direction means that a BCC lattice can be considered to be a special case of a hexagonal lattice (Figure 5). Supramolecular columns in the hexagonal lattice are defined as stacks of spheres aligned along the $[111]_{cub}$ direction (Figure 5a,b). Three distinct types of columns, denoted 1, 2, and 3 in Figure 5a,b,d, whose heights are displaced by $z = 0$, $c/3$, and $2c/3$, respectively, assemble into a $\sqrt{3} \times \sqrt{3}$ superlattice (Figure 5e and highlighted spheres in Figure 5b). The corner and center spheres of the BCC cell can then be defined by nine spheres, three from each of column types 1, 2, and 3 (Figure 5b,c). A more thorough mathematical treatment of the BCC phase as a special case of the hexagonal lattice is provided in the Supporting Information.

Columns Self-Organized from Supramolecular Spheres of G2-PBI. Consideration of a BCC phase as a special case of a hexagonal lattice (Figure 5) aids us in describing the supramolecular structure of G2-PBI in the 2D liquid crystalline columnar hexagonal phase with intracolumnar order (Φ_h^{io2}) observed between 125 and 158 °C. Superficially, XRD patterns of Φ_h^{io2} collected at 140 °C (Figure 6a) appear similar to those collected in the BCC phase at 180 °C (Figure 4a,b). However, azimuthal and radial plots (Figure 6c–e) show that peaks (1) and (4) are stronger and substantially sharper than peaks (2), (3), (5), and (6). Peaks (1) and (4) are true

DOI: 10.1021/jacs.6b09986
J. Am. Chem. Soc. 2016, 138, 14798–14807

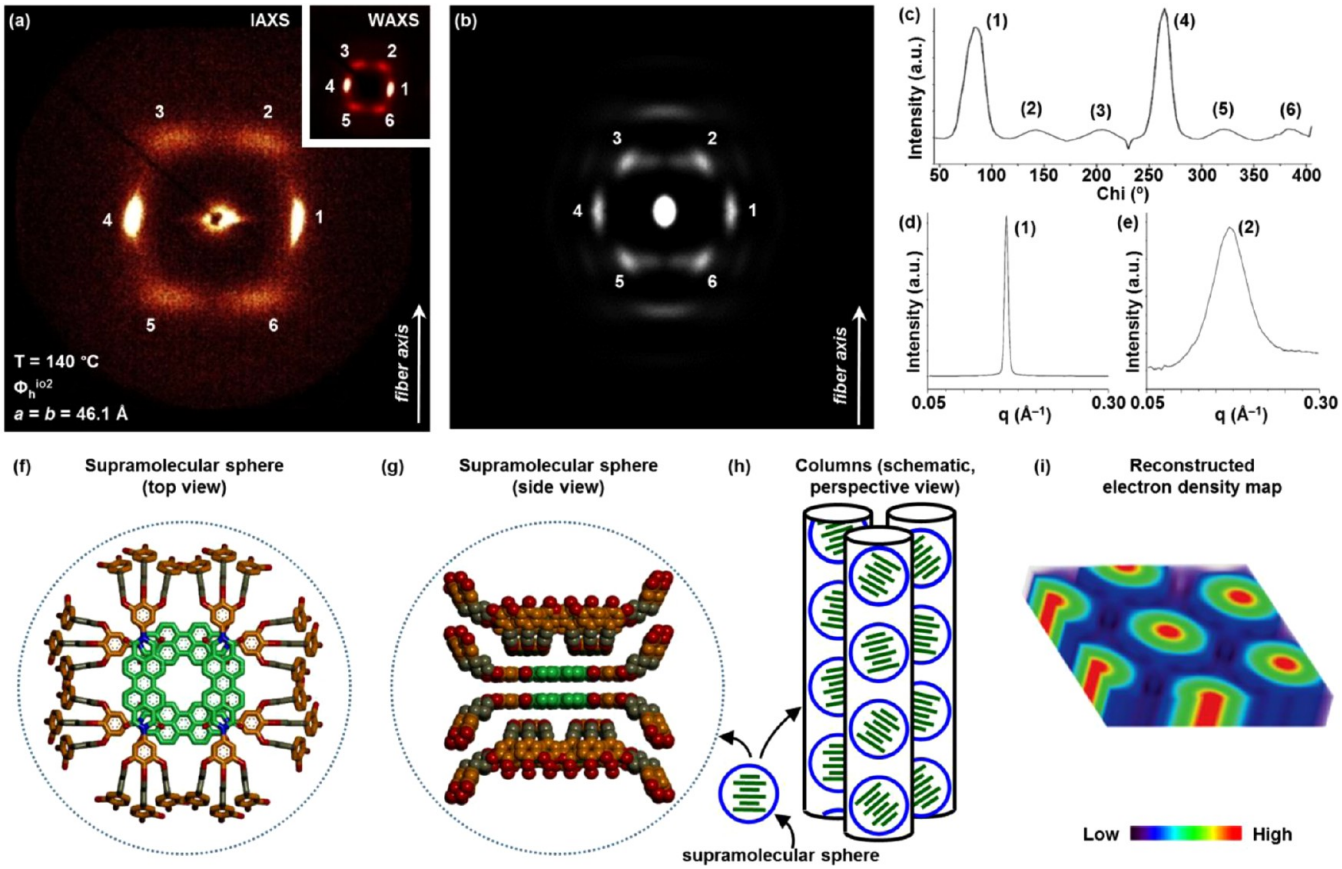

Figure 6. XRD patterns of the high temperature 2D liquid crystalline columnar hexagonal (Φ_h^{io2}) phase with intracolumnar order generated from supramolecular spheres. Data collected from an oriented fiber during first heating at 10 °C/min. (a) Experimental IAXS and (inset) WAXS patterns. (b) Simulation of fiber scattering from a hexagonal lattice in which supramolecular columns consist of spheres, as shown in Figure 5, with a single orientation of columns determined by the fiber axis. Temperature, phase, lattice parameters, and fiber axis are indicated. (c) Azimuthal plot of measured scattering intensity. Numerical labels correspond to those in (a). Fitted peak widths (full-width at half-maximum, fwhm) are (1) 16.2°, (2) 23.4°, (3) 21.0°, (4) 12.8°, (5) 20.4°, and (6) 21.6°. (d, e) Radial plots through (d) peak 1 (fwhm = 0.0032 Å^{-1}) and (e) peak 2 (fwhm = 0.058 Å^{-1}). (f) Top and (g) side views of the 12-molecule supramolecular sphere. Color code: O, red; N, blue; C atoms of the PBI, green; C atoms of phenyl rings, orange; C atoms of the propylene linker, gray. (h) Schematic representation of columns with molecules indicated as green bars. Peripheral dodecyl ($-C_{12}H_{25}$) chains are omitted for clarity. (i) Electron density map reconstructed from ($hk0$) Bragg peaks.

Bragg peaks, with radial width limited by instrumental resolution and azimuthal width limited by the orientational distribution of the fiber, while the other four peaks are strong diffuse maxima. The d-spacing of peaks (1) and (4) is 39.8 Å which, interpreted as the (100) diffraction of a hexagonal lattice (Figure 6i), would correspond to a hexagonal lattice parameter, a, and column diameter, D_{col} (= a) of 46.2 Å. The proposed space group of the Φ_h^{io2} phase is $P6mm$.

The strong similarity of the XRD pattern of Φ_h^{io2} (Figure 6a) to that of the BCC phase (Figure 4a,b) suggests a model for this intermediate phase. Peaks (1) and (4) in Figure 6a,b are at almost exactly the same positions as the (110) diffractions in the BCC phase (Figure 4a,b), but peaks (2), (3), (4), and (5), while nominally similar to (110) diffractions, are much broader, indicating the presence of disorder. Reconstructed electron density maps (Figure 6i) support a hexagonal arrangement of columns, but cannot provide information about the distribution of electron density along the column c-axis due to the lack of Bragg peaks with $l \neq 0$ observed by XRD. However, simulation of fiber scattering (Figure 6b) reproduces the experimental XRD pattern (Figure 6a) and demonstrates that columns composed of spheres along the $[111]_{cub}$ direction and randomly displaced along their long axis, can produce this diffraction peak broadening. Thus, the proposed structure of Φ_h^{io2} is similar to the hexagonal lattice depicted in Figure 5a, with 12-molecule spherical units (Figure 5f,g) packed into columns with only short-range *height*–*height* correlations between columns. Hence the same supramolecular sphere generated for the first time from a PBI is able to self-organize into a BCC phase (Figure 4) and also into a column of supramolecular spheres (Figure 6). Organization into columns of supramolecular spheres rather than disk shape building blocks is entropically favored[19] while also preserving favorable intersphere van der Waals interactions, thus providing a driving force for the formation of the Φ_h^{io2} phase. The structural analysis of the four phases of G2-PBI is summarized in Table 1.

Molecular Dynamics Investigated by Solid State ^{1}H and ^{13}C NMR. Solid state cross-polarization magic angle spinning (CP-MAS) NMR experiments interrogate both the structure and dynamics of chemical groups within supramolecular structures.[20] ^{13}C variable temperature (VT) CP-MAS NMR spectra (Figure 7b) are readily observed for G2-PBI in Φ_h^{io1}, demonstrating the low mobility of the PBI molecules in the columnar assemblies. Transition from Φ_h^{io1} to Φ_h^{io2} results in a continuous decrease in the intensity of the ^{13}C CP-MAS signals (compare Figure 7b, 100 °C with 120 and 140 °C). This

DOI: 10.1021/jacs.6b09986
J. Am. Chem. Soc. 2016, 138, 14798–14807

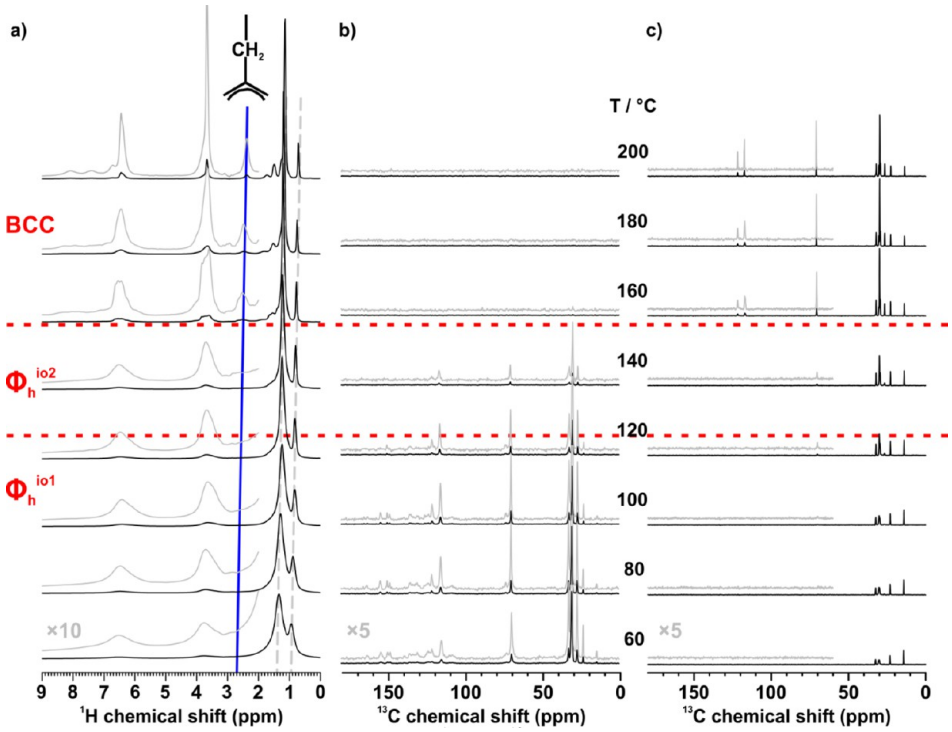

Figure 7. Solid state variable temperature (VT) ^{1}H and ^{13}C NMR spectra of G2-PBI recorded at 10 kHz MAS spinning frequency and 500 MHz ^{1}H Larmor frequency. (a) ^{1}H VT magic angle spinning (MAS) NMR spectra. (b) ^{13}C VT cross-polarization magic angle spinning (CP-MAS) NMR spectra. (c) ^{13}C VT insensitive nuclei enhanced by polarization transfer magic angle spinning (INEPT-MAS) NMR spectra.

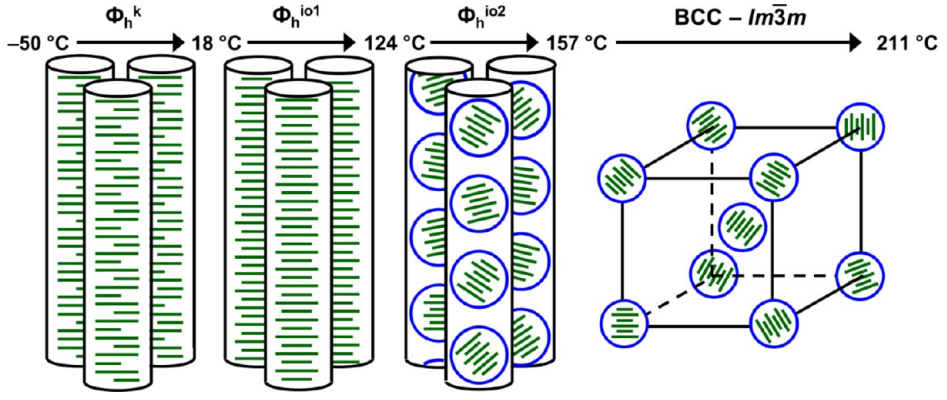

Figure 8. Schematic models of the four phases of G2-PBI. Phase notation: Φ_h^{k}, 3D crystalline columnar hexagonal phase; Φ_h^{io1}, low temperature 2D liquid crystalline columnar hexagonal phase with intracolumnar order; Φ_h^{io2}, high temperature 2D liquid crystalline columnar hexagonal phase with intracolumnar order; BCC ($Im\bar{3}m$), body-centered cubic phase. Transition temperatures as observed by DSC upon second heating at 10 °C/min are noted.

diminishing intensity indicates increasing motion of G2-PBI as the supramolecular spheres of the Φ_h^{io2} phase become increasing orientationally disordered. The disappearance of ^{13}C CP-MAS signals between 160 and 200 °C indicate that G2-PBI becomes so mobile in the BCC phase that heteronuclear dipolar couplings are absent (Figure 7b), and hence ^{13}C CP-MAS NMR spectra cannot be recorded.

In contrast, high resolution liquid state type ^{13}C insensitive nuclei enhanced by polarization transfer magic angle spinning (INEPT-MAS) NMR[21] monitors only those molecular sites where dipolar couplings between neighboring spins are sufficiently averaged by molecular motions to allow for T_2 relaxation times longer than 10 ms, and thus provides information complementary to, but inaccessible via, the CP-MAS measurement. ^{13}C INEPT-MAS NMR spectra (Figure 7c) demonstrate how the molecular mobility of G2-PBI increases with increasing temperature from the periphery of the molecule toward the core. A weak signal around 75 ppm is observed in the Φ_h^{io2} phase, suggestive of a greater degree of motion than in the INEPT-MAS-silent Φ_h^{io1} phase, and consistent with the introduction of some orientational disorder in the stacks of G2-PBI. At the phase transition from Φ_h^{io2} to the BCC phase, the outer phenyl rings of the dendrons, which show restricted molecular motions in Φ_h^{io2}, become mobile, as indicated by the increased INEPT-MAS NMR signal intensity (Figure 7c) and confirmed by the reduced CP-MAS NMR signal intensity (Figure 7b). This observation supports our interpretation that G2-PBI forms supramolecular objects which exhibit almost perfect columnar order in the Φ_h^{io2} phase but

DOI: 10.1021/jacs.6b09986
J. Am. Chem. Soc. 2016, 138, 14798−14807

have, on average, spherical symmetry in the BCC phase due to orientational averaging.

Pleasingly, ^{1}H MAS spectra (Figure 7a) are more easily interpreted. Just above the phase transition, at T = 160 °C (phase transition by DSC = 158 °C), the BCC phase becomes very heterogeneous, as indicated by the broad, almost rectangular, signals arising from the $-OCH_2$ protons of the linker between the inner and outer phenyl rings around 3.8 ppm and from the phenyl protons around 6.5 ppm and supported by 2D $^{1}H-^{13}C$ INEPT-MAS correlation NMR (Figure SF5). This observation indicates that the propyl linkers between the inner and the outer phenyl rings become mobile in the cubic phase. At higher temperature, these molecular fluctuations are sufficiently fast as to average heterogeneities on the time scale of the NMR experiment. All signals from the outer dendritic part of the molecules indicate a common shift toward lower ppm values with increasing temperature, which might be attributed to thermal expansion and the increasingly important entropic contributions of the dendritic side groups. Thus, solid state NMR studies show that this high order system exhibits a marked mobility, at its highest at the periphery of G2-PBI, which increases with temperature and changes at the phase transitions. This mobility provides the basis for the formation of spherically averaged units that can self-organize into a cubic lattice.

CONCLUSIONS

The structural and retrostructural analysis of the supramolecular assemblies of a PBI functionalized with two second generation self-assembling dendrons at its imide groups, G2-PBI, is summarized in Figure 8. G2-PBI adopts a new crown conformation which permits assembly into a crystalline columnar hexagonal (Φ_h^k) phase via asymmetric tetrameric crowns (TCs) and a 2D liquid crystalline columnar hexagonal (Φ_h^{io1}) phase with intracolumnar order via symmetric TCs. Above 124 °C, G2-PBI has sufficient molecular mobility to allow inversion of TCs and formation of an unprecedented supramolecular sphere. This is the first example known to us of a supramolecular sphere generated from a PBI derivative. This sphere self-organizes into a BCC phase rarely observed for self-assembling dendrons but favorable here due to the compact, nondeformable nature of the isotropic spheres generated by G2-PBI.[19] Upon cooling, a columnar hexagonal (Φ_h^{io2}) phase in which supramolecular columns are unexpectedly made of spheres is formed. We propose that the conformational flexibility inherent in G2-PBI which permits rapid molecular motion at higher temperature is critical to its ability to self-assemble into a supramolecular sphere. We anticipate that the spheres and BCC phase of G2-PBI will provide general design principles for the assembly of additional molecular building blocks into spherical supramolecular units and their subsequent self-organization into further 3D structures. The hierarchical mechanism of self-organization of supramolecular spheres and periodic arrays generated from them will be shown to be general with libraries of PBIs and of other related planar molecules. The transition from the periodic arrays generated from spheres to the array generated from classical columns is expected to provide access to a new generation of molecular switches.

ASSOCIATED CONTENT

Supporting Information

The Supporting Information is available free of charge on the ACS Publications website at DOI: 10.1021/jacs.6b09986.

Experimental procedures with complete characterization data and additional discussion (PDF)

AUTHOR INFORMATION

Corresponding Author

*percec@sas.upenn.edu

Notes

The authors declare no competing financial interest.

ACKNOWLEDGMENTS

Financial support by the National Science Foundation (DMR-1066116 (V.P.), DMR-1120901 (V.P. and P.A.H.), and OISE-1243313 (VP)), the Humboldt Foundation (V.P.) and the P. Roy Vagelos Chair at Penn (V.P.) are gratefully acknowledged. X.Z. acknowledges support from the joint NSF-EPSRC PIRE project "RENEW" (EPSRC Grant EP-K034308). B.E.P. thanks the Howard Hughes Medical Institute for an International Student Research Fellowship. The authors thank Dr. Qi Xiao for assistance with optical polarized microscopy.

REFERENCES

(1) For recent reviews on assemblies of PBIs, see: (a) Würthner, F.; Saha-Möller, C. R.; Fimmel, B.; Ogi, S.; Leowanawat, P.; Schmidt, D. *Chem. Rev.* **2016**, *116*, 962−1052. (b) Rosen, B. M.; Wilson, C. J.; Wilson, D. A.; Peterca, M.; Imam, M. R.; Percec, V. *Chem. Rev.* **2009**, *109*, 6275−6540. (c) Wöhrle, T.; Wurzbach, I.; Kirres, J.; Kostidou, A.; Kapernaum, N.; Litterscheidt, J.; Haenle, J. C.; Staffeld, P.; Baro, A.; Giesselmann, F.; Laschat, S. *Chem. Rev.* **2016**, *116*, 1139−1241.

(2) (a) Krieg, E.; Bastings, M. M. C.; Besenius, P.; Rybtchinski, B. *Chem. Rev.* **2016**, *116*, 2414−2477. (b) Görl, D.; Würthner, F. *Angew. Chem., Int. Ed.* **2016**, *55*, 12094−12098. (c) Thota, B. N. S.; Urner, L. H.; Haag, R. *Chem. Rev.* **2016**, *116*, 2079−2102.

(3) (a) Anthony, J. E.; Facchetti, A.; Heeney, M.; Marder, S. R.; Zhan, X. *Adv. Mater.* **2010**, *22*, 3876−3892. (b) Facchetti, A. *Chem. Mater.* **2011**, *23*, 733−758. (c) Huang, C.; Barlow, S.; Marder, S. R. *J. Org. Chem.* **2011**, *76*, 2386−2407. (d) Tsarfati, Y.; Strauss, V.; Kuhri, S.; Krieg, E.; Weissman, H.; Shimoni, E.; Baram, J.; Guldi, D. M.; Rybtchinski, B. *J. Am. Chem. Soc.* **2015**, *137*, 7429−7440. (e) Shahar, C.; Dutta, S.; Weissman, H.; Shimon, L. J. W.; Ott, H.; Rybtchinski, B. *Angew. Chem., Int. Ed.* **2016**, *55*, 179−182. (f) Hartnett, P. E.; Margulies, E. A.; Matte, H. S. S. R.; Hersam, M. C.; Marks, T. J.; Wasielewski, M. R. *Chem. Mater.* **2016**, *28*, 3928−3936. (g) Gsänger, M.; Bialas, D.; Huang, L.; Stolte, M.; Würthner, F. *Adv. Mater.* **2016**, *28*, 3615−3645. (h) Ogi, S.; Stepanenko, V.; Thein, J.; Würthner, F. *J. Am. Chem. Soc.* **2016**, *138*, 670−678. (i) Fernandez-Ariza, J.; Krick Calderon, R. M.; Rodriguez-Morgade, M. S.; Guldi, D. M.; Torres, T. *J. Am. Chem. Soc.* **2016**, *138*, 12963−12974.

(4) For early examples of columnar liquid crystalline assemblies of PBIs, see: (a) Cormier, R. A.; Gregg, B. A. *Chem. Mater.* **1998**, *10*, 1309−1319. (b) Würthner, F.; Thalacker, C.; Diele, C.; Tschierske, C. *Chem. - Eur. J.* **2001**, *7*, 2245−2253. (c) An, Z.; Yu, J.; Jones, S. C.; Barlow, S.; Yoo, S.; Domercq, B.; Prins, P.; Siebbeles, L. D. A.; Kippelen, B.; Marder, S. R. *Adv. Mater.* **2005**, *17*, 2580−2583. (d) Debije, M. G.; Chen, Z.; Piris, J.; Neder, R. B.; Watson, M. M.; Müllen, K.; Würthner, F. *J. Mater. Chem.* **2005**, *15*, 1270−1276. (e) Chen, Z.; Baumeister, U.; Tschierske, C.; Würthner, F. *Chem. - Eur. J.* **2007**, *13*, 450−465.

(5) For selected examples of structural studies on PBI assemblies from our laboratory, see: (a) Percec, V.; Peterca, M.; Tadjiev, T.; Zeng, X.; Ungar, G.; Leowanawat, P.; Aqad, E.; Imam, M. R.; Rosen, B. M.; Akbey, U.; Graf, R.; Sekharan, S.; Sebastiani, D.; Spiess, H. W.; Heiney,

DOI: 10.1021/jacs.6b09986
J. Am. Chem. Soc. 2016, 138, 14798−14807

P. A.; Hudson, S. D. *J. Am. Chem. Soc.* **2011**, *133*, 12197−12219. (b) Percec, V.; Hudson, S. D.; Peterca, M.; Leowanawat, P.; Aqad, E.; Graf, R.; Spiess, H. W.; Zeng, X.; Ungar, G.; Heiney, P. A. *J. Am. Chem. Soc.* **2011**, *133*, 18479−18494. (c) Percec, V.; Sun, H.-J.; Leowanawat, P.; Peterca, M.; Graf, R.; Spiess, H. W.; Zeng, X.; Ungar, G.; Heiney, P. A. *J. Am. Chem. Soc.* **2013**, *135*, 4129−4148. (d) Roche, C.; Sun, H.-J.; Leowanawat, P.; Araoka, F.; Partridge, B. E.; Peterca, M.; Wilson, D. A.; Prendergast, M. E.; Heiney, P. A.; Graf, R.; Spiess, H. W.; Zeng, X.; Ungar, G.; Percec, V. *Nat. Chem.* **2016**, *8*, 80−89.

(6) (a) Balagurusamy, V. S. K.; Ungar, G.; Percec, V.; Johansson, G. *J. Am. Chem. Soc.* **1997**, *119*, 1539−1555. (b) Hudson, S. D.; Jung, H.-T.; Percec, V.; Cho, W.-D.; Johansson, G.; Ungar, G.; Balagurusamy, V. S. K. *Science* **1997**, *278*, 449−452.

(7) Yeardley, D. J. P.; Ungar, G.; Percec, V.; Holerca, M. N.; Johansson, G. *J. Am. Chem. Soc.* **2000**, *122*, 1684−1689.

(8) Ungar, G.; Liu, Y.; Zeng, X.; Percec, V.; Cho, W.-D. *Science* **2003**, *299*, 1208−1211.

(9) Zeng, X.; Ungar, G.; Liu, Y.; Percec, V.; Dulcey, A. E.; Hobbs, J. K. *Nature* **2004**, *428*, 157−160.

(10) (a) Bates, F. S.; Fredrickson, G. H. *Phys. Today* **1999**, *52*, 32−38. (b) Lee, S.; Bluemle, M. J.; Bates, F. S. *Science* **2010**, *330*, 349−353. (c) Choi, S.-H.; Bates, F. S.; Lodge, T. P. *Macromolecules* **2014**, *47*, 7978−7986. (d) Lee, S.; Leighton, C.; Bates, F. S. *Proc. Natl. Acad. Sci. U. S. A.* **2014**, *111*, 17723−17731. (e) Gillard, T. M.; Lee, S.; Bates, F. S. *Proc. Natl. Acad. Sci. U. S. A.* **2016**, *113*, 5167−5172. (f) Chanpuriya, S.; Kim, K.; Zhang, J.; Lee, S.; Arora, A.; Dorfman, K. D.; Delaney, K. T.; Fredrickson, G. H.; Bates, F. S. *ACS Nano* **2016**, *10*, 4961−4972. (g) Arora, A.; Qin, J.; Morse, D. C.; Delaney, K. T.; Fredrickson, G. H.; Bates, F. S.; Dorfman, K. D. *Macromolecules* **2016**, *49*, 4675−4690.

(11) (a) Weber, R. L.; Ye, Y.; Schmitt, A. L.; Banik, S. M.; Elabd, Y. A.; Mahanthappa, M. K. *Macromolecules* **2011**, *44*, 5727−5735. (b) Sorenson, G. P.; Schmitt, A. K.; Mahanthappa, M. K. *Soft Matter* **2014**, *10*, 8229−8235. (c) Perroni, D. V.; Mahanthappa, M. K. *Soft Matter* **2013**, *9*, 7919−7922. (d) Perroni, D. V.; Baez-Cotto, C. M.; Sorenson, G. P.; Mahanthappa, M. K. *J. Phys. Chem. Lett.* **2015**, *6*, 993−998.

(12) (a) Huang, M.; Hsu, C.-H.; Wang, J.; Mei, S.; Dong, X.; Li, Y.; Li, M.; Liu, H.; Zhang, W.; Aida, T.; Zhang, W.-B.; Yue, K.; Cheng, S. Z. D. *Science* **2015**, *348*, 424−428. (b) Zhang, W.; Huang, M.; Su, H.; Zhang, S.; Yue, K.; Dong, X.-H.; Li, X.; Liu, H.; Zhang, S.; Wesdemiotis, C.; Lotz, B.; Zhang, W.-B.; Li, Y.; Cheng, S. Z. D. *ACS Cent. Sci.* **2016**, *2*, 48−54.

(13) (a) Zhang, X.; Chen, Z.; Würthner, F. *J. Am. Chem. Soc.* **2007**, *129*, 4886−4887. (b) Zhang, X.; Rehm, S.; Safont-Sempere, M. M.; Würthner, F. *Nat. Chem.* **2009**, *1*, 623−629. (c) Görl, D.; Zhang, X.; Würthner, F. *Angew. Chem., Int. Ed.* **2012**, *51*, 6328−6348.

(14) Sun, H.-J.; Zhang, S.; Percec, V. *Chem. Soc. Rev.* **2015**, *44*, 3900−3923.

(15) (a) Percec, V.; Imam, M. R.; Peterca, M.; Wilson, D. A.; Heiney, P. A. *J. Am. Chem. Soc.* **2009**, *131*, 1294−1304. (b) Percec, V.; Imam, M. R.; Peterca, M.; Wilson, D. A.; Graf, R.; Spiess, H. W.; Balagurusamy, V. S. K.; Heiney, P. A. *J. Am. Chem. Soc.* **2009**, *131*, 7662−7677.

(16) Rosen, B. M.; Wilson, D. A.; Wilson, C. J.; Peterca, M.; Won, B. C.; Huang, C.; Lipski, L. R.; Zeng, X.; Ungar, G.; Heiney, P. A.; Percec, V. *J. Am. Chem. Soc.* **2009**, *131*, 17500−17521.

(17) Percec, V.; Peterca, M.; Dulcey, A. E.; Imam, M. R.; Hudson, S. D.; Nummelin, S.; Adelman, P.; Heiney, P. A. *J. Am. Chem. Soc.* **2008**, *130*, 13079−13094.

(18) (a) Heiney, P. A.; Fischer, J. E.; McGhie, A. R.; Romanow, W. J.; Denenstein, A. M.; McCauley, J. P., Jr.; Smith, A. B.; Cox, D. E. *Phys. Rev. Lett.* **1991**, *66* (22), 2911−2914. (b) Michel, K. H.; Copley, J. R. D.; Neumann, D. A. *Phys. Rev. Lett.* **1992**, *68* (19), 2929−2932.

(19) Li, Y.; Lin, S.; Goddard, W. A., III *J. Am. Chem. Soc.* **2004**, *126*, 1872−1885.

(20) (a) Hansen, M. R.; Graf, R.; Spiess, H. W. *Acc. Chem. Res.* **2013**, *46*, 1996−2007. (b) Hansen, M. R.; Graf, R.; Spiess, H. W. *Chem. Rev.* **2016**, *116*, 1272−1308.

(21) Nowacka, A.; Bongartz, N. A.; Ollila, O. H. S.; Nylander, T.; Topgaard, D. *J. Magn. Reson.* **2013**, *230*, 165−175.

DOI: 10.1021/jacs.6b09986
J. Am. Chem. Soc. 2016, 138, 14798−14807